Hindawi
Geofluids
Volume 2022, Article ID 3889950, 9 pages
https://doi.org/10.1155/2022/3889950

Research Article

Influence of Water-Resisting Layer Thickness on Fracture Evolution in Karst Tunnel and Control Measures

Chun Liu and Congying Jiang

School of Civil Engineering and Architecture, Zhejiang Guangsha Vocational and Technical University of Construction, Dongyang 322100, China

Correspondence should be addressed to Congying Jiang; jiangcy@zjgsdx.edu.cn

Received 13 January 2022; Revised 6 February 2022; Accepted 11 February 2022; Published 7 March 2022

Academic Editor: Feng Xiong

In this paper, a series of studies are carried out on the hidden karst encountered in the excavation of Baziling tunnel. In this paper, the safe thickness of the water-resisting layer in a hidden karst cave and tunnel is studied by means of engineering geological investigation, numerical simulation, and neural network. The numerical calculation model is established through the geological survey. Innovate to use BP neural network and differentiation algorithm to inverse the rock mechanical parameters. By analyzing the influence of different thicknesses of the water-resisting layer on the deformation and failure of surrounding rock, the final thickness of the water-resisting layer is obtained. At the same time, the influence of water pressure on the thickness of the water-resisting layer is studied, and the treatment scheme under different water pressure is finally determined.

1. Introduction

Karst water inrush does great harm to tunnel construction. The development of the karst cave causes the instability of tunnel surrounding rock and the disaster of water and mud inrush, which is difficult to control. In the prediction of karst water inflow, many scholars at home and abroad have conducted extensive research, but there is little research on the safe thickness in front of the tunnel [1]. Li et al. [2] proposed an accurate and feasible systematic evaluation method for water inrush risk of karst tunnel. The confidence criterion is used to judge the risk level of water inrush. The calculation results of this method are compared with an example. The comparison results show that the evaluation results of this method are basically consistent with the field observation results. Li et al. [3] established a water inrush risk assessment software system by comprehensively considering 8 risk factors, such as groundwater level, unfavorable geology, formation lithology, terrain, formation dip angle, excavation, advanced geological prediction, and monitoring. Wang et al. [4] combined the weighting method with the normal cloud model and proposed a new water inrush evaluation method. Specifically, the evaluation index system is established, and each index is quantitatively divided into four levels. A comprehensive weighting algorithm is proposed, which combines the analytic hierarchy process, entropy method, and the statistical method to reasonably allocate index weight. Lin et al. [5] combined variable weight theory with cloud model theory to construct a calculation model for karst tunnel construction risk assessment.

Based on the extension evaluation method, Zhang et al. [6] proposed an improved water inrush risk evaluation system for carbonate karst tunnel. The system considers karst geological conditions and selects 9 main factors affecting tunnel water inrush as evaluation indexes. According to the value of the evaluation index or expert judgment, the evaluation index is quantitatively divided into four risk levels. Wang et al. [7] proposed a risk assessment method for water inrush and water inrush interval of karst tunnel. On this basis, the concept and calculation form of the risk assessment models are proposed, and the risk environment, construction factors, and feedback information are analyzed. Zhao et al. [8] classified the water and mud gushing of railway tunnels according to a large number of examples of

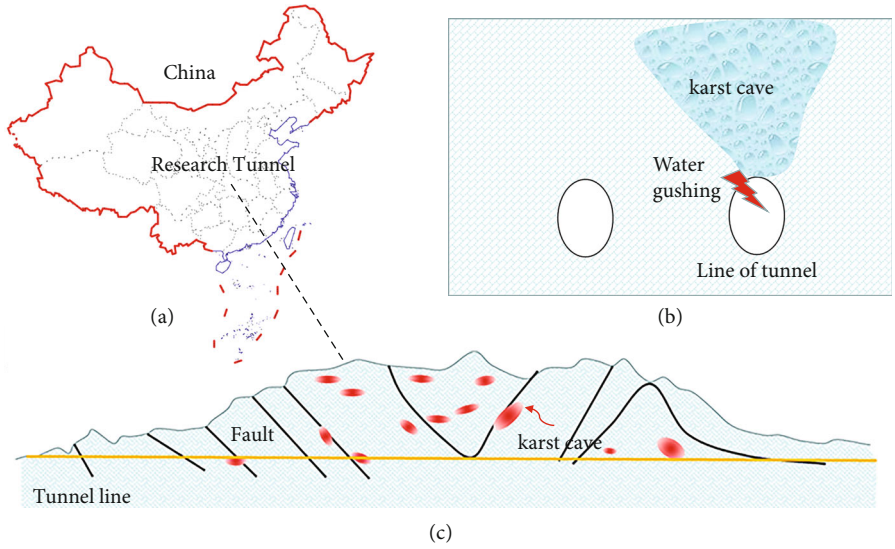

Figure 1: Overview of research target tunnel.

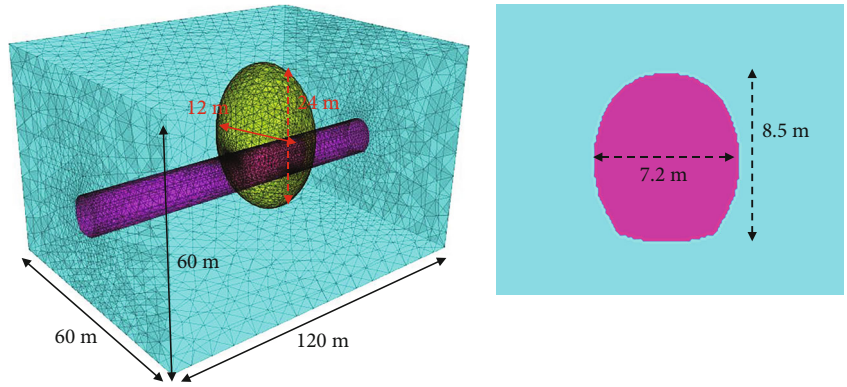

(a) Numerical calculation model (b) Tunnel excavation profile

Figure 2: Numerical calculation model.

water and mud gushing of the railway tunnels, combined with the surrounding rock conditions and meteorological factors of tunnel excavation. Combined with the macro and micro mechanisms, the causes of water inrush and mud inrush are summarized, and the targeted treatment methods are put forward. The treatment methods include selecting the advanced geological prediction method according to the risk degree of different sections of the tunnel, determining the prediction items, and selecting the appropriate methods, namely, drainage guidance method, blockage guidance method, or drainage blockage method. Li et al. [9] analyzed the transformation mechanism of water inrush and seepage caused by excavation disturbance and analyzed the potential water-bearing area of the tunnel by using the electromagnetic geophysical exploration method. The constitutive model of rock mass and grouting parameters is considered in the numerical simulation. The initiation and propagation laws of tunnel cracks under different curtain grouting parameters are put forward. The characteristics of seepage and water inrush caused by tunnel excavation are described. It is considered that the seepage characteristics of tunnel can be divided into incubation stage, sudden stage, and stable stage.

Liu et al. [10] selected a specific project and introduced the geological conditions, water inrush, mud inrush disasters, and subsequent prevention and control countermeasures. Then, the original grouting design and process as well as 25 grouting cycles and field operation of excavation are introduced to evaluate the grouting effect and suggestions for future grouting work. Based on the field investigation, the values of main grouting parameters are put forward. The grouting thickness is 5~8 m, the grouting length is 15~18 m (3~3.6 times the thickness), and the grouting amount per meter is 34.2 m^3. Wang et al. [11] proposed a new method of real-time monitoring and fusion early warning of tunnel water inrush. Zhu et al. [12] proposed a fuzzy comprehensive evaluation method for water inrush risk of tunnel water rich fault based on grey theory. The grey fuzzy method consists of two parts: one is the single factor evaluation matrix established by the evaluation index and the risk

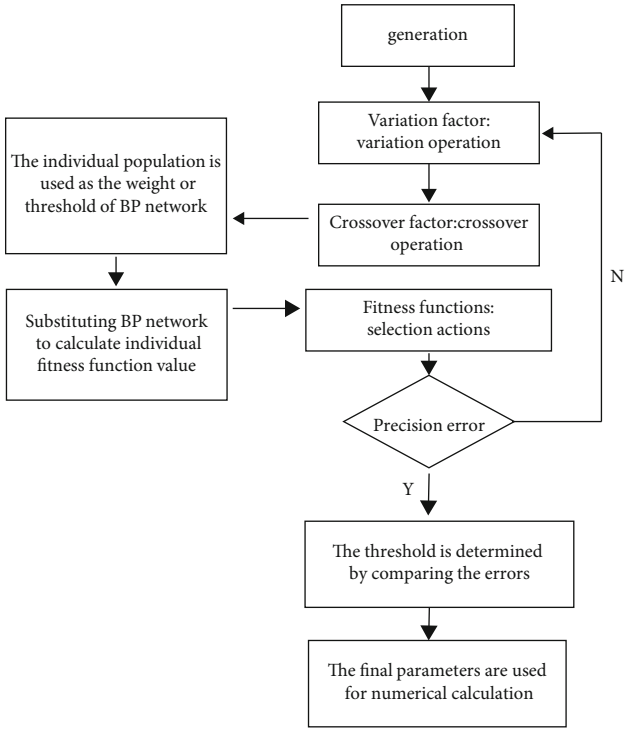

Figure 3: Algorithm flowchart.

grade membership function, and the other is to determine the weight of each evaluation index by using the norm grey correlation degree. From the aspects of formation lithology, geological structure, and hydrogeological conditions, five influencing factors such as fault dip angle, groundwater level, RMR, permeability, and formation dip angle are selected as evaluation indexes. Huang et al. [13] proposed a numerical method to study the influence of fractures on fluid flow, considering different types of discontinuities. The conceptual model of fractured water inrush focusing on the evolution of fracture connectivity is established, the seepage process of fluid in fractured rock mass is studied, and then, the water inrush mechanism is studied.

In tunnel engineering in karst area, when there are large karst caves in tunnel excavation, the checking calculation of tunnel safety thickness will be a key problem in engineering practice. The selection of its safe thickness is directly related to the project cost and project quality. Selecting an appropriate safe thickness will produce huge economic and social benefits for the whole project. However, due to many factors involved, there is no reliable analysis method for checking the safe thickness of the tunnel. In this paper, the influence of different isolation safety thickness on seepage is discussed by using the methods of engineering geological investigation, theoretical analysis, and numerical calculation. The reasonable safe thickness is determined, and the relevant advance grouting scheme is designed.

2. Engineering Geological Characteristics

2.1. Project Overview. Baziling tunnel of Yichang Wanzhou railway is located in Yesanguan Town, Changyang County, Yichang City, Hubei Province, China, with a design speed of 160 km/h, as shown in Figure 1. The total length of the tunnel is 5867 m, one side uphill, and the maximum buried depth is 695 m. The tunnel is located at the junction of the Yangtze River system, with dalupo syncline, jianshanling anticline, and chuanxinping syncline developed. The tunnel consists of Silurian, Devonian, Triassic, and Quaternary. The length of limestone stratum is 4464 m. The length of Silurian and Devonian fragments is 1550 m. Tunnel layer, two underground river systems around the tunnel. The area where most strata of the tunnel pass through is densely covered with karst and underground rivers are developed. The normal water inflow of the tunnel is 73000 m^3/d. The maximum water inflow is 302000 m^3/d.

2.2. Typical Karst Cave Characteristics. The revealed karst direction of DK 0+104 is NE80°, and the karst cavity gradually shrinks to both ends to form a fault structure. It is developed vertically, almost upright, and large-scale eroded stalactite suspension is developed upward and downward, with a small amount of dripping water. DK108+835.5 karst cave is 3 m long, 3.5 m wide, and 6 m high along the strike, filled with mud and stone, and collapsed during excavation. DK108+831 karst cave is 4.5 m wide, which is limestone, with relatively developed joint fissures, nearly horizontal karst cavity, vertical fissures, and relatively broken. The width of DK108+955 karst cavity is 6.2 m, and the karst cave is 4.5 m away from the top excavation contour line. The occurrence of some rocks in the karst cave is nearly horizontal, with vertical cracks and relatively broken. Dk108+698 dissolution fissure, 3 m in the transverse direction, 1.5 m in the longitudinal direction, and about 2.0 m high, gradually decreases upward, and the filling of the karst cave collapses. The filling is soil mixed with stone without water. Dk108 +683 crevice karst cave runs through the tunnel face, with a width of about 2.0 m. The filler is mud mixed with stone. The vertical joints around the karst cave are developed, with a joint spacing of about 2 m. The surrounding rock at the tunnel arch is relatively broken. DK109+039 reveals a fissured karst cave, which runs through more than 80% of the tunnel face from the left side of the line, is 1.0 m wide, soil mixed with stone, there is no water, and the fissures in the surrounding rock around the karst cave are developed. DK109+089 karst is about 1 m wide and 2.5 m deep. It runs along the tunnel line and is about 3 m long. The filling is clay with slight water seepage. The surrounding rock around the karst cave is broken, and there is a huge dangerous rock at the arch.

3. Numerical Calculation Model

3.1. Establish Numerical Calculation Model. The discrete element numerical calculation software is used for modeling, and the influence of model boundary is fully considered [14–16]. The model size is 60 m ∗ 60 m ∗ 120 m. The tunnel excavation contour span is 7.2 m, the height is 8.5 m, and the thickness of the secondary lining is 50 cm, as shown in Figure 2. The karst cave is simplified as an ellipsoid, with a long axis of 24 m and a short axis of 14 m. The karst cave

Table 1: Mechanical parameters of optimized rock mass.

Limestone rock parameters	Density (kg/m^3)	E (GPa)	Poisson's ratio	Cohesion (MPa)	Internal friction angle (°)	Tensile strength (MPa)
	2500	10	0.25	12	35	11
Limestone joint parameters	Normal stiffness (GPa)	Tangential stiffness (GPa)	Internal friction angle (°)			
	10	10	30			

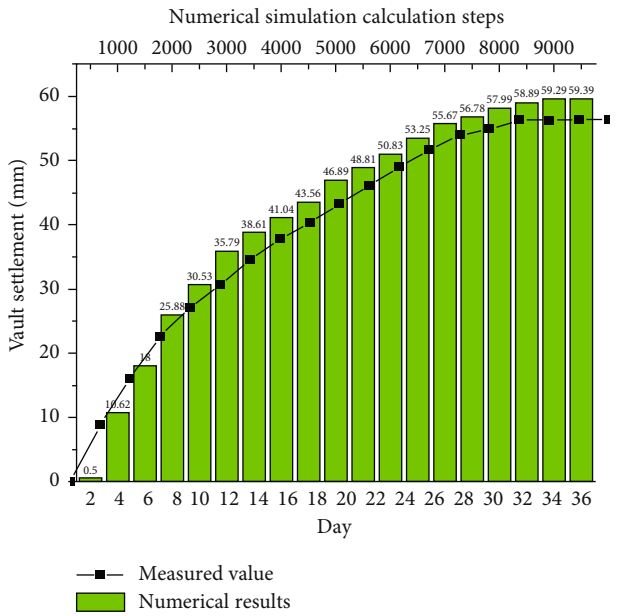

Figure 4: Comparison between numerical simulation and measured settlement of tunnel vault.

is located in front of the tunnel. The buried depth of the simulated tunnel is 600 m; the vertical stress only considers the unit weight of rock mass. The geological survey report shows that the study area lateral pressure coefficient is 1.4 under the influence of fault. The x-direction boundary, y-direction boundary, and z-direction boundary of the model are constrained by normal displacement. The water pressure inside the karst cavity acts directly on the interface.

3.2. Constitutive Model. The block element adopts a unified strength constitutive model, which considers the different effects of all stress components acting on the double shear element on the yield or failure of materials [17–21]. It is suitable for all kinds of tensile and compressive materials and is a collection of a series of linear strength criteria. The expression of principal stress of unified strength theory is the most widely used, which can directly reflect the influence of each principal stress on material strength. The expression of the principal stress form of unified strength theory is

$$\text{if } \sigma_2 \le \frac{\sigma_1 + \alpha\sigma_3}{1+\alpha}, \quad F = \sigma_1 - \frac{\alpha}{1+\mathrm{b}}(b\sigma_2 + \sigma_3) = f_t, \tag{1}$$

$$\text{if } \sigma_2 \ge \frac{\sigma_1 + \alpha\sigma_3}{1+\alpha}, \quad F' = \frac{1}{1+\mathrm{b}}(\sigma_1 + b\sigma_2) - \alpha\sigma_3 = f_t, \tag{2}$$

$$\alpha = \frac{(1-\sin\varphi)}{(1+\sin\varphi)}, \tag{3}$$

$$f_t = \frac{2c\cos\varphi}{(1+\sin\varphi)}. \tag{4}$$

In the formula, $\sigma_1, \sigma_2, \sigma_3$ represents the maximum principal stress, the intermediate principal stress, and the minimum principal stress, respectively; f_t is uniaxial tensile strength; α is tension compression strength ratio; b is the unified strength theoretical parameter, and $0 \le b \le 1$. c is cohesion and φ is internal friction angle. Coulomb sliding joint model can fully represent the joint shear failure, tension crack failure, compression shear failure, and tension shear failure in rock mass [22, 23]. In the elastic deformation stage of joints, the stress of joints follows

$$T_{\max} = -TA_c, \tag{5}$$

$$F^s_{\max} = cA_c + F^n \tan\varphi. \tag{6}$$

In the formula, F^n is the normal force; T is tensile strength; c is cohesion; φ is the internal friction angle.

The joint seepage in numerical calculation obeys the law of legislation. The expression is shown in

$$q = \frac{ge^3}{12v}J. \tag{7}$$

In the formula, q is the unit area seepage flow per unit time; J is hydraulic gradient; e is the crack opening; g is gravitational acceleration; v is the viscosity coefficient of water flow; when the water temperature is 15°, $v = 1.14 * 10^{-6}$ m^2/s.

3.3. Calculation Parameter Value. The field test and laboratory test cannot effectively determine the mechanical parameters of complex geotechnical media. Due to its nonuniformity, cracks, and other factors, the results of mechanical parameters have great randomness and limitations, and there is a large error with the field measured values. In order to make up for the shortcomings of the above methods, this paper uses the geotechnical back analysis method to obtain the parameter value in the numerical calculation [24, 25].

In this paper, the combination of BP neural network and differential evolution algorithm is used for inverse analysis to establish the nonlinear relationship between surrounding rock displacement and mechanical parameters as shown in

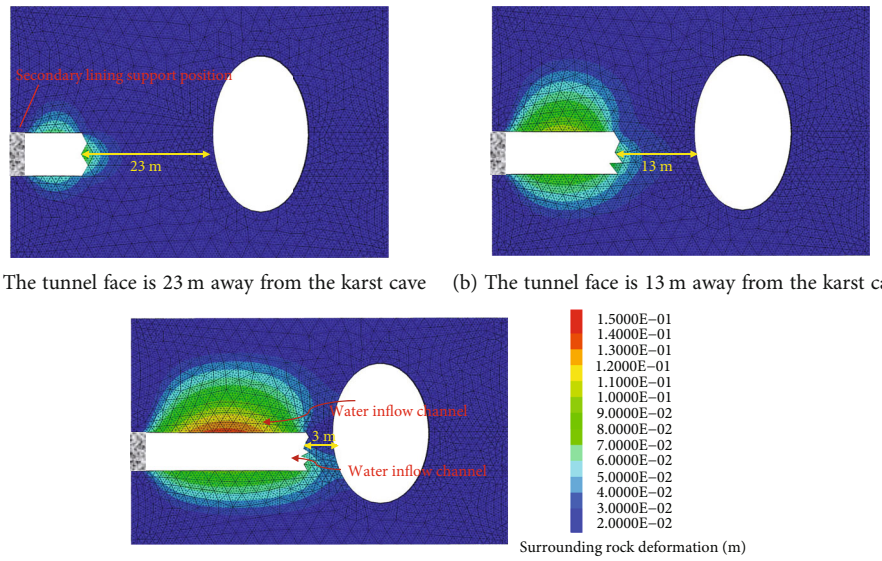

(a) The tunnel face is 23 m away from the karst cave (b) The tunnel face is 13 m away from the karst cave

(c) The tunnel face is 3 m away from the karst cave

Figure 5: Deformation characteristics of surrounding rock under different thickness of water-resisting layer.

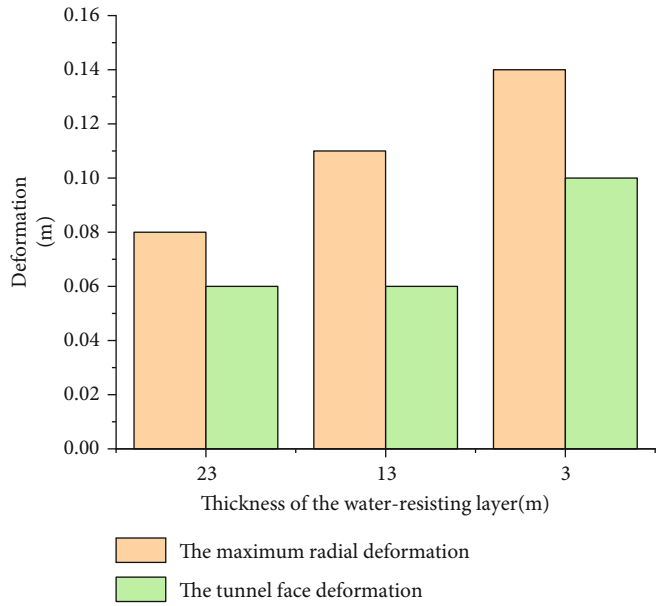

Figure 6: Deformation of tunnel under different thickness of water-resisting layer.

Figure 3. BP neural network is a complex and nonlinear dynamic analysis system, including input layer, hidden layer, and output layer. The network response corresponding to the input mode is transmitted from the input layer to the output layer through the middle layer. According to the error between the actual tunnel displacement value and the numerical simulation value, the connection weight is corrected from the output layer to the input layer through the hidden layer so that the difference between the actual value and the expected value is gradually reduced. However, BP neural network has some problems, such as slow convergence speed, poor network performance, uncertain learning rate, and easy to fall into local minimum. Different evolution can make up for the shortcomings of BP neural network. Differential evolution algorithm simulates the evolution of biological population and iterates repeatedly, so as to retain the individuals who meet the adaptation conditions. It retains the global search ability of genetic algorithm and has the robustness and strong global optimization ability.

Taking the surrounding rock parameters as the input layer vector and the displacement value as the output layer vector, the rock elastic modulus E, cohesion c, and internal friction angle φ are selected; joint shear stiffness k_s, joint normal stiffness k_n, joint internal friction angle k_φ, and joint

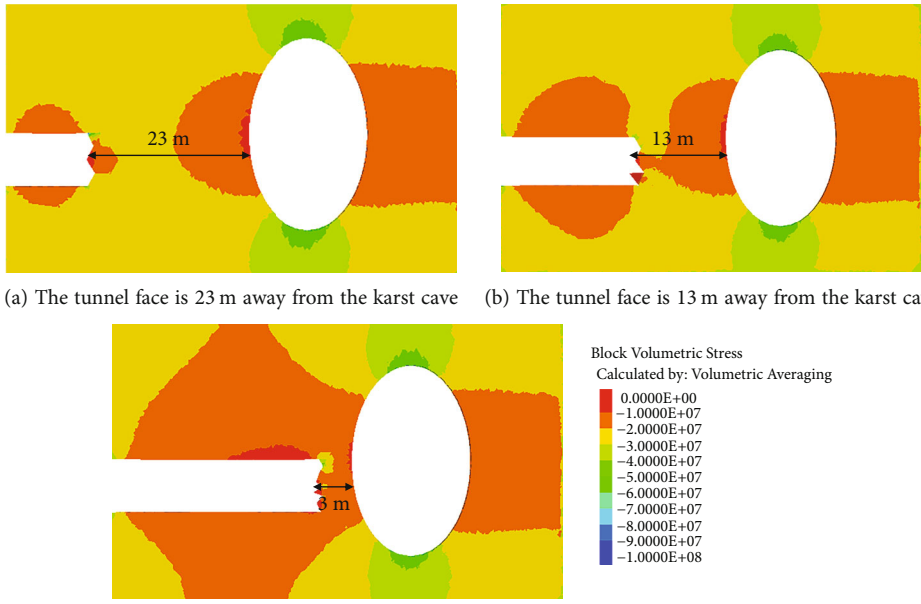

(a) The tunnel face is 23 m away from the karst cave (b) The tunnel face is 13 m away from the karst cave

(c) The tunnel face is 3 m away from the karst cave

Figure 7: Block volumetric stress of surrounding rock under different thickness of water-resisting layer.

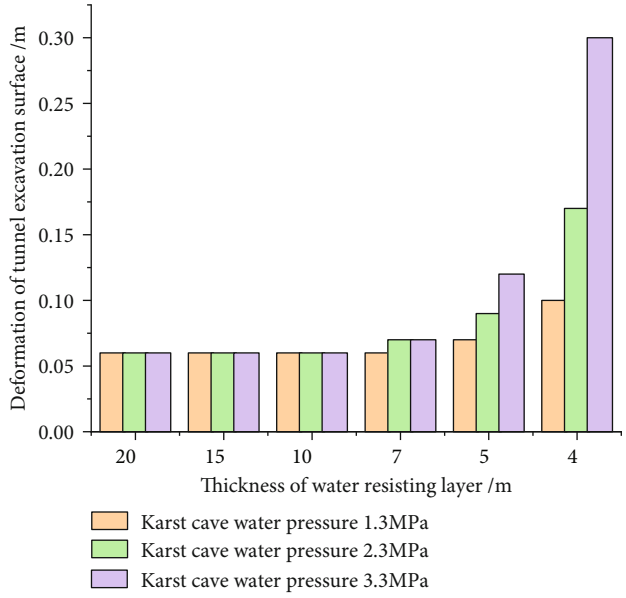

Figure 8: Displacement and deformation characteristics of tunnel face under different water pressure.

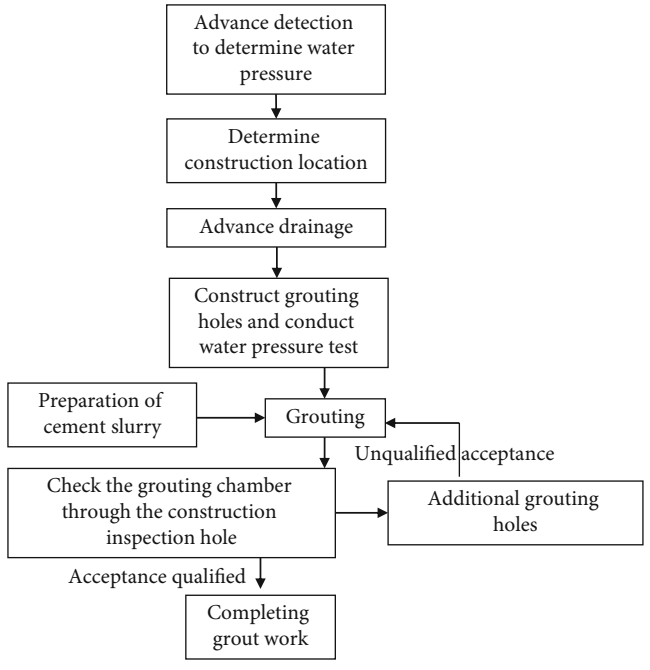

Figure 9: Curtain grouting process flowchart.

cohesion k_c are the input parameters, and the numerical simulation displacement value is the output parameter. The parameters shown in Table 1 are used to compare the measured value with the simulation value, as shown in Figure 4. The numerical calculation and analysis show that the calculation step is balanced at 9500 steps, and the maximum settlement of the arch crown is 59.39 m. The measured results show that the maximum settlement of arch crown is 55.3 mm, and the stability time is about 31 days after excavation. The numerical simulation can fully reflect the deformation characteristics of the surrounding rock, and the parameters obtained from inversion can be used for subsequent research.

4. Analysis of Numerical Results

4.1. Deformation Characteristics. Figures 5 and 6 show the influence of different water-resisting layer thicknesses on surrounding rock deformation and seepage when the water pressure in the karst cave is 2.3 MPa. The calculation shows that with the continuous advancement of the tunnel, the deformation and failure of surrounding rock are mainly

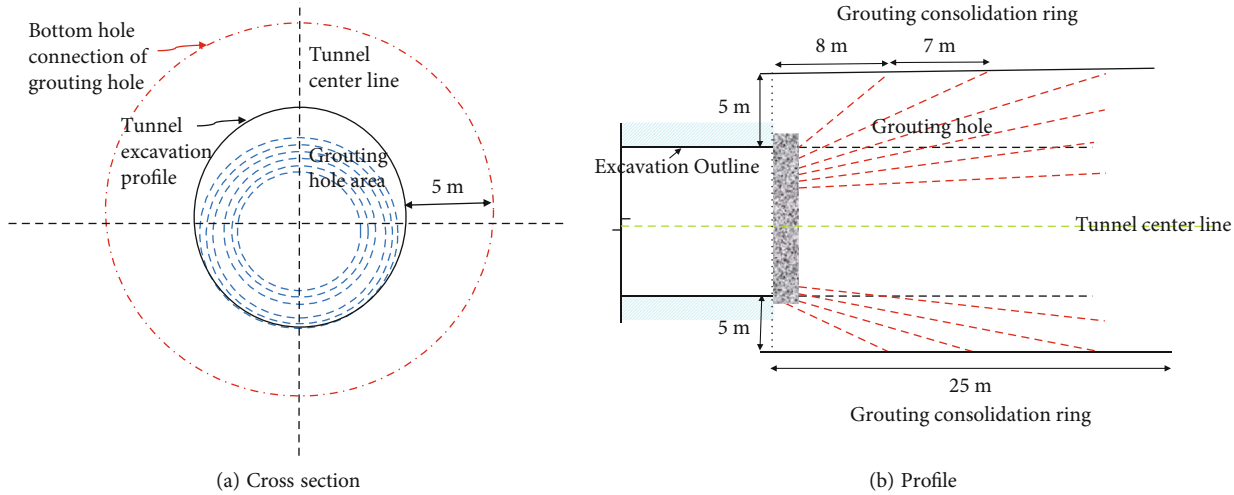

(a) Cross section (b) Profile

Figure 10: Design drawing of advance curtain grouting.

divided into two parts: radial development and advanced influence, and the radial deformation increases with the extension of the distance from the secondary lining. When 9 m away from the secondary lining, the thickness of the water-resisting layer is 23 m, the maximum radial deformation is 0.08 m, the tunnel face deformation is 0.06 m, and the advanced influence distance is 10 m. When 19 m away from the secondary lining, the thickness of the water-resisting layer is 13 m, the maximum radial deformation is 0.11 m, the tunnel face deformation remains 0.06 m, and the advance influence distance is 10 m. When 29 m away from the second lining, the thickness of the water-resisting layer is 3 m, the maximum radial deformation is 0.14 m, the maximum deformation of the tunnel face surges to 0.1 m, and a seepage channel is generated with the karst cave. The water in the solution cavity flows into the tunnel through the seepage channel, resulting in disasters. With the decrease of the safe thickness of the water-resisting layer, the advance stress caused by tunnel excavation is superimposed and coupled with the stress concentration around the karst cave, resulting in damage. Therefore, in order to ensure safe production, it is necessary to control the distance between the secondary lining and the tunnel face, analyze the minimum water-resisting layer thickness under different water pressure conditions, and advance grouting before reaching the minimum water-resisting layer thickness.

As shown in Figure 7, it shows the variation law of volume stress with the decrease of the thickness of the water-resisting layer during tunnel excavation. Volume stress can fully show the three-dimensional stress state of the unit body. With the decrease of the thickness of the water-resisting layer, the low stress area caused by tunnel excavation is fused with the low stress area caused by karst cave, which is easy to form a seepage channel.

4.2. Influence of Water Pressure in Karst Cave on Safe Thickness. When the water pressure of the karst cave is 1.3 MPa, 2.3 MPa, and 3.3 MPa, respectively, the displacement of excavation surface is shown in Figure 8. When the thickness of the water-resisting layer is more than 10 m, the change of water pressure in the karst cave has no impact on the tunnel face, and the deformation is 0.06 m. When the thickness of the water-resisting layer is 7 m, the water pressure is 2.3 MPa to 3.3 MPa, and the deformation increases by 25% compared with 1 MPa. When the thickness of the water-resisting layer is 5 m, it can be seen that the deformation increases sharply with the increase of water pressure. When the water pressure is 3.3 MPa, the deformation reaches 0.125 m. When the thickness of the water-resisting layer is 4 m and the water pressure is 3.3 MPa, the maximum deformation reaches 0.3 m. When the water pressure is 2.3 MPa, the deformation reaches 0.17 m. When the water pressure is 1.3 MPa, the deformation reaches 0.1 m. According to the above research, in order to ensure the safety of the tunnel during tunneling, the thickness of the water-resisting layer should be kept above 10 m, and then, the construction should be carried out by grouting in advance.

5. Control Measures and Effects

Advance drainage and curtain grouting are adopted for karst cave treatment to reduce water pressure and prevent outburst. Determine the water pressure in the karst cave according to the advanced geophysical exploration. When the water pressure is greater than 3.3 MPa, drainage and curtain grouting shall be carried out 10 m in advance. When the water pressure is greater than 2.3 MPa, drainage and curtain grouting shall be carried out 8 m in advance. When the water pressure is greater than 1.3 MPa, drainage and curtain grouting shall be carried out 6 m in advance. The treatment process flow is shown in Figure 9. Firstly, the solution cavity position and water pressure are determined by advanced geophysical exploration, so as to analyze the advanced control distance. Advance drilling shall be carried out to remove water pressure and curtain grouting shall be carried out.

The mixture of cement and water glass is used as grouting material. The water cement ratio of cement slurry is 1 : 1~1 : 1.5, the water glass concentration is 30~40 Baume degree, the cement water glass volume ratio is 1 : 0.3~1 : 1, and an appropriate amount of retarder is added as required.

The dosage is determined by test, generally 1%~3% of the dosage of cement. Through the analysis of the revealed geological conditions, after the advance curtain grouting construction is completed, the slurry fills the cracks more densely, reduces the formation permeability coefficient, and plays an effective role in water plugging.

Figure 10 shows the design of advance grouting, in which the advance reinforcement section is 25 m long. The thickness of grout stop wall is 2 m. The lateral reinforcement range is 5 m outside the contour line of the tunnel face. The slurry diffusion radius is 2.0 m. The spacing of final holes shall not exceed 3.0 m.

6. Conclusion

The stability of rock stratum between tunnel and karst cave is one of the main problems endangering safety in tunnel construction in karst area. During the construction of the tunnel through the karst area, the existing karst cave often leads to local collapse, block falling and rock falling during the tunnel excavation, especially the hidden karst cave that is not exposed during the excavation. Because the safety measures cannot be taken in advance, it is easy to be damaged out of guard, causing great potential safety hazards and great harm to the tunnel construction and operation. At present, there is a lack of systematic research on the impact of karst cave on tunnel construction in karst area. Therefore, it is necessary to systematically study the impact of karst cave on tunnel construction and explore its regularity, so as to carry out targeted treatment or pretreatment of karst cave in construction, ensuring the safety of tunnel construction in karst area. This paper studies the reasonable thickness of tunnel excavation surface and karst tunnel aquifuge and discusses the basic control methods. The specific conclusions are as follows:

(1) Through geological investigation and analysis, it is considered that the karst caves in the tunnel are densely distributed and the water content is huge. Therefore, the discrete element numerical calculation model is established, the unified constitutive model is adopted for the block, and the Coulomb slip model is adopted for the joint

(2) The method of back analysis of surrounding rock mechanical parameters through displacement is realized through neural network. It is considered that the combination of BP neural network and differential evolution algorithm can effectively reduce the simulation error

(3) When the water pressure is 1.3 MPa, the thickness of the water-resisting layer is too small, the deformation of the tunnel face increases sharply, and a seepage channel is generated with the karst cave. The advance stress caused by tunnel excavation is superimposed and coupled with the stress concentration around the karst cave, resulting in damage

(4) The increase of water pressure makes the thickness of the safety water-resisting layer increase accordingly. It is more reasonable to carry out advance grouting design according to different water pressure

Data Availability

The data used to support the findings of the study are available within the article.

Conflicts of Interest

The authors declare that they have no conflicts of interest.

Acknowledgments

This research was supported by the Project of Zhejiang Provincial Education Department (FX2019112).

References

[1] L. Li, W. Tu, S. Shi, J. Chen, and Y. Zhang, "Mechanism of water inrush in tunnel construction in karst area," *Geomatics, Natural Hazards and Risk*, vol. 7, no. sup1, pp. 35–46, 2016.

[2] S. Li, Z. Zhou, L. Li, Z. H. Xu, Q. Q. Zhang, and S. S. Shi, "Risk assessment of water inrush in karst tunnels based on attribute synthetic evaluation system," *Tunnelling and Underground Space Technology*, vol. 38, pp. 50–58, 2013.

[3] L. Li, T. Lei, S. Li et al., "Risk assessment of water inrush in karst tunnels and software development," *Arabian Journal of Geosciences*, vol. 8, no. 4, pp. 1843–1854, 2015.

[4] X. Wang, S. Li, Z. Xu, J. Hu, D. Pan, and Y. Xue, "Risk assessment of water inrush in karst tunnels excavation based on normal cloud model," *Bulletin of Engineering Geology and the Environment*, vol. 78, no. 5, pp. 3783–3798, 2019.

[5] C. Lin, M. Zhang, Z. Zhou et al., "A new quantitative method for risk assessment of water inrush in karst tunnels based on variable weight function and improved cloud model," *Tunnelling and Underground Space Technology*, vol. 95, p. 103136, 2020.

[6] K. Zhang, W. Zheng, C. Xu, and S. Chen, "An improved extension system for assessing risk of water inrush in tunnels in carbonate karst terrain," *KSCE Journal of Civil Engineering*, vol. 23, no. 5, pp. 2049–2064, 2019.

[7] X. Wang, S. Li, Z. Xu, X. Li, P. Lin, and C. Lin, "An interval risk assessment method and management of water inflow and inrush in course of karst tunnel excavation," *Tunnelling and Underground Space Technology*, vol. 92, p. 103033, 2019.

[8] Y. Zhao, P. Li, and S. Tian, "Prevention and treatment technologies of railway tunnel water inrush and mud gushing in China," *Journal of Rock Mechanics and Geotechnical Engineering*, vol. 5, no. 6, pp. 468–477, 2013.

[9] G. Li, W. Ma, S. Tian, Z. Hongbo, F. Huabin, and W. Zou, "Groundwater inrush control and parameters optimization of curtain grouting reinforcement for the Jingzhai tunnel," *Geofluids*, vol. 2021, 10 pages, 2021.

[10] J. Q. Liu, K. V. Yuen, W. Z. Chen, X. S. Zhou, and Wei-Wang, "Grouting for water and mud inrush control in weathered granite tunnel: a case study," *Engineering Geology*, vol. 279, p. 105896, 2020.

[11] S. Wang, L. Li, S. Cheng et al., "Study on an improved real-time monitoring and fusion prewarning method for water inrush in tunnels," *Tunnelling and Underground Space Technology*, vol. 112, p. 103884, 2021.

[12] B. Zhu, L. Wu, Y. Peng, W. Zhou, and C. Chen, "Risk assessment of water inrush in tunnel through water-rich fault," *Geotechnical and Geological Engineering*, vol. 36, no. 1, pp. 317–326, 2018.

[13] Z. Huang, K. Zhao, X. Li, W. Zhong, and Y. Wu, "Numerical characterization of groundwater flow and fracture-induced water inrush in tunnels," *Tunnelling and Underground Space Technology*, vol. 116, p. 104119, 2021.

[14] G. C. Shi, X. J. Yang, H. C. Yu, and C. Zhu, "Acoustic emission characteristics of creep fracture evolution in double- fracture fine sandstone under uniaxial compression," *Engineering Fracture Mechanics*, vol. 210, pp. 13–28, 2019.

[15] C. Zhu, M. C. He, B. Jiang, X. Z. Qin, Q. Yin, and Y. Zhou, "Numerical investigation on the fatigue failure characteristics of water-bearing sandstone under cyclic loading," *Journal of Mountain Science*, vol. 18, no. 12, pp. 3348–3365, 2021.

[16] G. Li, Y. Hu, S. M. Tian, M. Weibin, and H. L. Huang, "Analysis of deformation control mechanism of prestressed anchor on jointed soft rock in large cross-section tunnel," *Bulletin of Engineering Geology and the Environment*, vol. 80, no. 12, pp. 9089–9103, 2021.

[17] M. Z. Gao, J. Xie, Y. N. Gao et al., "Mechanical behavior of coal under different mining rates: a case study from laboratory experiments to field testing," *International Journal of Mining Science and Technology*, vol. 31, no. 5, pp. 825–841, 2021.

[18] M. Z. Gao, H. C. Hao, S. N. Xue et al., "Discing behavior and mechanism of cores extracted from Songke-2 well at depths below 4,500 m," *International Journal of Rock Mechanics and Mining Sciences*, vol. 149, p. 104976, 2022.

[19] C. Cao, W. Zhang, J. Chen, B. Shan, S. Song, and J. Zhan, "Quantitative estimation of debris flow source materials by integrating multi- source data: a case study," *Engineering Geology*, vol. 291, p. 106222, 2021.

[20] D. Chen, H. Chen, W. Zhang, J. Lou, and B. Shan, "An analytical solution of equivalent elastic modulus considering confining stress and its variables sensitivity analysis for fractured rock masses," *Journal of Rock Mechanics and Geotechnical Engineering*, vol. 2021, 2021.

[21] H. Liang, L. Wang, D. Xuaning, H. Wen, X. Yuan, and W. Zhang, "Similarity quantification of soil parametric data and sites using confidence ellipses," *Geoscience Frontiers*, vol. 13, no. 1, article 101280, 2022.

[22] C. Zhu, M. Karakus, M. He, Q. Meng, and Y. C. Yuan, "Flexural toppling mechanism and stability analysis of an anti-dip rock slope," *Rock Mechanics and Rock Engineering*, vol. 54, no. 8, pp. 3721–3735, 2021.

[23] B. D. Ding, Z. Y. Han, G. C. Zhang et al., "Volumetric deformation and damage evolution of Tibet interbedded skarn under multistage constant-amplitude-cyclic loading," *International Journal of Rock Mechanics and Mining Sciences*, vol. 152, p. 105066, 2022.

[24] Z. Dou, S. X. Tang, X. Y. Zhang et al., "Influence of shear displacement on fluid flow and solute transport in a 3D rough fracture," *Lithosphere*, vol. 2021, no. Special 4, p. 1569736, 2021.

[25] Z. Dou, Y. M. Liu, X. Y. Zhang et al., "Influence of layer transition zone on rainfall-induced instability of multilayered slope," *Lithosphere*, vol. 2021, no. Special 4, p. 2277284, 2021.